Research paper

Comparing variance of signal contained in the most recent GRACE solutions

Artur Lenczuk[1]*, Grzegorz Leszczuk[2], Anna Klos[3], Janusz Bogusz[4]

Faculty of Civil Engineering and Geodesy, Military University of Technology, Warsaw, Poland
[1]e-mail: artur.lenczuk@wat.edu.pl; ORCID: http://orcid.org/0000-0002-9573-1302

[2]e-mail: grzegorz.leszczuk@student.wat.edu.pl; ORCID: http://orcid.org/0000-0001-6920-3429

[3]e-mail: anna.klos@wat.edu.pl; ORCID: http://orcid.org/0000-0001-6742-8077

[4]e-mail: janusz.bogusz@wat.edu.pl ORCID: http://orcid.org/0000-0002-0424-7022

*Corresponding author: Artur Lenczuk

Abstract: Gravity Recovery and Climate Experiment (GRACE) mission data is widely used in various fields of science. GRACE explored changes of the gravity field regularly from April 2002 to June 2017. In the following research, we examine variance of signal contained in two different formats of GRACE data: standard spherical harmonics and mass concentration blocks (so-called "mascons") solutions, both provided in the most recent releases. For spherical harmonics-based solution, we use monthly gravity field solutions provided up to degree and order (d/o) 96 by three different computing centers, i.e. the NASA's Jet Propulsion Laboratory (JPL), the German Research Center for Geosciences (GFZ) and the Center for Space Research (CSR). For the mass concentration blocks, we use values of total water storage provided by the CSR, JPL and the Goddard Space Flight Center (GSFC) computing centers, which we convert to spherical harmonic coefficients up to d/o 96. We show that using the anisotropic DDK3 filter to smooth the north-south stripes present in total water storage obtained from standard spherical harmonics solution leaves more information than common isotropic Gaussian filter. In the case of mascons, GSFC solution contains much more information than the CSR and JPL releases, relevant for corresponding d/o. Differences in variance of signal arise from different background models as well as various shape and size of mascons used during processing of GRACE observations.

Keywords: GRACE, degree variance, spherical harmonic coefficients, mass concentration blocks

1. Introduction

Various satellite gravity missions enable that variations of the global gravity field are reliably estimated (Wahr et al., 2006; Bouman and Fuchs, 2012; Bruinsma et al., 2010;

Save et al., 2012; Rexer et al., 2014). As the gravity field varies temporarily and spatially due to the change in the distribution of masses either inside or on the surface of the Earth, a continuous information on gravity is needed to monitor these changes in different temporal and spatial scales. Monthly information on global gravity variance has been successfully provided by the Gravity Recovery and Climate Experiment (GRACE; Tapley et al., 2004). The key instrument of the GRACE satellite mission is the K-Band Ranging system (KBR; Cheng and Tapley, 2004). The KBR system provides precise measurements of the distance between the GRACE A and B satellites. From the KBR low-low satellite to satellite tracking (SST) and the high-low GPS (Global Positioning System) and GRACE twin satellites tracking, the monthly fluctuations in gravity fields are determined. GRACE satellites enabled the estimates of Global Geopotential Models (GGMs) for 15 years, i.e. since April 2002 to June 2017, providing an enormous global dataset for Earth sciences (Wang et al., 2017a), including cryosphere (Chen et al., 2006; Luthcke et al., 2008; 2013), ocean mass variability (Chambers and Bonin, 2012) or studying post-seismic displacements (Han et al., 2008). Most importantly, temporal variations of hydrological masses determined from GRACE satellite mission data agreed perfectly with the corresponding ones obtained from hydrological models (Bruinsma et al., 2010; Rodell et al., 2018; Scanlon et al., 2018) and altimetric datasets (Forsberg et al., 2017), yielding also a great opportunity to estimate global hydrological cycle or a sea-level budget (Loomis et al., 2019).

The GRACE satellite mission data are available as Level-0, Level-1, Level-2 or Level-3 products, depending on the computing centers. GRACE observations are processed and archived in a Science Data System (Tapley et al., 2004). Level-0 products constitute a raw data, received twice per day from each satellite. Then, to develop Level-1 products, the GRACE intersatellite ranges are processed independently by few computing centers, which use various corrections, parameter choices and solution strategies (Sakumura et al., 2014). At this stage, data products needed for further processing are also provided, i.e. Level-1B Atmosphere and Ocean De-aliasing product – AOD1B. After calibration and validation of GRACE Level-1B products, Level-2 products are provided by several centers. They include temporal, i.e. weekly/monthly, and static (mean), gravity fields. Level-2 products are most often employed by users, since they characterize monthly changes of the geopotential field in the form of spherical harmonic coefficients to degree and order (d/o) 60/96 or in the form of gridded Total Water Storage (*TWS*) values provided for mass concentration blocks (so-called "mascons"). Level-3 products are the most user-friendly. These include gridded ready-to-use values, which definitely simplifies analyses performed on gravity fields. GRACE data, apart from their various forms, differ also in solution strategies, choice of the input parameters and gravitational force, mean geopotential, ocean, atmospheric and solid Earth tides as well as ocean pole tides. Nevertheless, continuous improvement of background models and new gravitational force estimates results in new releases launched by computing centers for both GRACE data forms: spherical harmonic coefficients (which we refer to as "GRACE-based GGMs") and mascon solutions. GRACE-based GGMs are characterized by north-south stripes in the final model of gravity field. Stripes occur as a result of poor ob-

servability of the gravity gradient towards east-west for near-polar orbits (Kundu, 2016; Feng, 2019) or as an artifact due to the oversampling of the Earth's static disturbing potential (Peidou and Pagiatakis, 2020). Hence, GRACE-based GGMs have to be initially pre-processed to reduce noise. Mascons are constructed in such a way that signal is concentrated in the location of each mascon cell. This guarantees that the north-south stripes are already filtered out (or smoothed) (Luthcke et al., 2013; Watkins et al., 2015, Save et al., 2016) and the signal leakage between land and ocean is reduced (Rowlands et al., 2010). Several studies proved a good agreement between these two forms of GRACE data in terms of global changes. However, for regional studies, mascons have been shown to better represent small-scale mass changes than the GRACE-based GGMs (Sabaka et al., 2010; Luthcke et al., 2013; Save et al., 2016).

Several studies focused on a degree variance analysis between available GRACE solutions showing more significant restrictions of signal for GRACE-based GGMs than for mascons (e.g. Watkins et al., 2015, Save et al., 2016; Loomis et al., 2019). Comparative studies of both forms of GRACE solutions were based on analyses of changes in *TWS* and proved that *TWS* determined from mascon solution correlate better with the corresponding ones obtained from hydrological models than those estimated from GRACE-based GGMs (Andrews et al., 2014; Scanlon et al., 2016; Nair and Indu, 2018; Zhou et al., 2018). Nowadays, more and more studies are based on mascon solutions, which contain more signal information than GRACE-based GGMs (Scanlon et al., 2016) and do not need any pre-processing to be applied.

In this research, we assess monthly GRACE data depending on the solution and the computing center they are provided by. The research questions read as follows: "What is the variance of signal contained in both types of GRACE data provided by different computing centers? What is the impact of various spatial filtering methods and data types on the reduction of noise and signal loss?". To answer these questions, we use a square root of degree variance statistics examining the signal information contained in each degree and order of spherical harmonic coefficients. The article is organized in such a way that the two types of GRACE data used and the methods implemented for the degree variance estimates are described in Sections 2 and 3, respectively. The results are presented in Section 4. Section 5 summarizes our research.

2. Data

2.1. Spherical harmonic coefficients (GRACE-based GGMs)

We use spherical harmonic coefficients C_{nm} and S_{nm} provided within the release 6.0 (RL06) of GRACE-based GGMs developed recently by three different GRACE computing centers: the CSR (Center for Space Research, Austin) (Bettadpur, 2018), GFZ (German Research Center for Geosciences, Potsdam) (Dahle et al., 2018) and JPL (Jet Propulsion Laboratory, California) (Dah-Ning, 2018). GRACE-based GGMs provided by these computing centers differ mostly by the background models employed during the processing, such as the mean gravity field model, the atmosphere and ocean de-aliasing models and tidal oceanic models. Additionally, we also employ degree-1 and

degree-2 corrections. Degree-1 spherical harmonic coefficients are replaced using the methodology presented by Sun et al. (2016). Degree-2 spherical harmonic coefficients are replaced by Satellite Laser Ranging (SLR) estimates. Moreover, the Glacial Isostatic Adjustment (GIA) effect was removed using the ICE5-G (Peltier, 2004) and A Geruo et al. (2013) models. Table 1 presents summarized information of background models used by each computing center.

Table 1. Background models used by the CSR, GFZ and JPL computing centers to process GRACE observations which are then provided as the spherical harmonic coefficients. We replaced two spherical harmonic coefficients: (1) degree-1 spherical harmonic coefficients are replaced by the combination of GRACE data and geophysical models with the method presented by Sun et al. (2016), and (2) degree-2 spherical harmonic coefficients are replaced by the corresponding ones obtained from Satellite Laser Ranging (SLR) estimates

Background models	GRACE analysis center		
	CSR	GFZ	JPL
Mean (static) gravity field	GGM05C	EIGEN-6C4	GSM05C
3rd body ephemerides	IERS2010	IERS2010	IERS2010
Atmosphere and ocean de-aliasing	AOD1B_RL06 (ECMWF+MPIOM)	AOD1B_RL06 (ECMWF+MPIOM)	AOD1B_RL06 (ECMWF+OMCT)
Ocean tides	GOT4.8+SCEQ	FES2014b+SCEQ	FES2014b+SCEQ
Solid Earth and pole tides	IERS2010	IERS2010	IERS2010
Degree-1 spherical harmonic coefficients	coefficients based on ocean and atmospheric models and GRACE coefficients for degrees 2 and higher (TN13a; Sun et al., 2016)	coefficients based on ocean and atmospheric models and GRACE coefficients for degrees 2 and higher (TN13b; Sun et al., 2016)	coefficients based on ocean and atmospheric models and GRACE coefficients for degrees 2 and higher (TN13c; Sun et al., 2016)
Degree-2 spherical harmonic coefficients	coefficients replaced using SLR estimates (TN11; Cheng and Ries, 2017)	coefficients replaced using SLR estimates (TN11; Cheng and Ries, 2017)	coefficients replaced using SLR estimates (TN11; Cheng and Ries, 2017)

The north-south stripes present in GRACE-based GGMs cause that the noise increases at higher degrees of spherical harmonic coefficients. We examine the effectiveness of two different noise filtering methods: the isotropic Gaussian filter (Wahr et al., 1998) and the anisotropic decorrelation filter DDK3 (Kusche, 2007; Kusche et al., 2009). For Gaussian filtering, we employ spatial smoothing using 300 km radii, which corresponds to similar smoothing range as is provided using the DDK3 filter.

For the CSR and GFZ centers, we employ monthly GRACE-based GGMs up to d/o 96 from April 2002 to June 2017 (163 months in total). For the JPL center, a number of 161 months of GRACE solutions are available up to d/o 96 from April 2002 to June 2017. These are supplemented with 2 months of data for January and February 2015 up to d/o 60 (163 months in total).

2.2. Mass concentration blocks (mascons)

Mascon solutions are a relatively new form for gravity changes representation, which is defined as mass concentration blocks on a sphere (Muller and Sjögren, 1968). For these blocks, a specific density value is assumed. Mascons are provided by three GRACE computing centers, i.e. by the CSR and JPL centers, and by the GSFC (Goddard Space Flight Center, Maryland) center. Mascon solutions provided by individual computing centers differ by processing variants, as well as sizes, shapes and spatial resolutions of blocks on a sphere.

Mascon solution provided in the newest release RL06 by the CSR computing center are defined on a grid with a spatial resolution of $0.25°$, in the shape of $40\,950$ hexagons and 12 pentagons. Each mascon corresponds to the tiles $\sim$120 km wide or size of $1°$ on the equator resulting in $41\,000$ equal areas ($12\,400$ km^2). Signal leakage between land and ocean is narrowed using the Root Mean Square (RMS) signal values computed from GRACE-based GGMs. Additionally, the noise is reduced by applying constrains, which are based only on GRACE observations (Save et al., 2016). Monthly CSR mascons are available from April 2002 to June 2017 (163 months in total) with spatial range between $89.875°$N to $89.875°$S for latitude and $0.125°$E to $359.875°$E for longitude. For the background models, the CSR analysis center applies the GGM05C mean gravity field model and DE430 planetary ephemerides. Atmosphere and ocean de-aliasing effects were removed by the European Centre for Medium-Range Weather Forecast (ECMWF) and Max-Planck-Institute for Meteorology Ocean Model (MPIOM) models. Ocean tides were accounted for using GOT4.8 model with the Self-Consistent EQuilibrium model (SCEQ, Ray et al., 1994). The GIA effect is reduced using ICE6G_D model (Peltier et al., 2018).

Mascon solution provided in the newest release RL06 by the JPL computing center are defined on a grid with a spatial resolution of $0.5°$. The gravity field is parametrized using $3° \times 3°$ grid cells, which corresponds to a native resolution of $\sim$330 km at the equator. In total, $4\,551$ circle cells distributed globally are provided (Watkins et al., 2015). Signal leakage between land and ocean is reduced by the CRI (Coastline Resolution Improvement) method (Watkins et al., 2015). Furthermore, mascon constraints are based on both GRACE observations and geophysical models, i.e. ocean and terrestrial hydrology models. Monthly solutions are available from April 2002 to June 2017 (163 months in total) with spatial range between $89.75°$N to $89.75°$S for latitude and $0.25°$E to $359.75°$E for longitude. As the background models, the GIF48 mean gravity field model and DE421 planetary ephemerides were used. Atmosphere and ocean de-aliasing effects were removed by the ECMWF and Ocean Model for Circulation and Tides (OMCT) model. Ocean tides were accounted for using the GOT4.7 model with SCEQ model. The GIA effect is reduced using the ICE6G_D model (Peltier et al., 2018).

The most recent mascon solution provided by the GSFC defines mascons in a form of $41\,168$ squares on a grid with a spatial resolution of $1°$, which corresponds to ~110 km at the equator resulting in $12\,390$ km^2 equal areas (Luthcke et al., 2013). They were constructed with an adaptive decomposition filter using anisotropic constraints to estimate global mass change. Furthermore, the least squares method was used to enforce spatial

restrictions (Luthcke et al., 2013), which significantly improved the signal-to-noise ratio for this solution (Loomis et al., 2019). Monthly solution is available from January 2003 to July 2016 (148 months in total) with spatial range between 90°N to 90°S for latitude and 0.5°E to 359.5°E for longitude. During GSFC mascon calculation, the GOCO-05S mean gravity field model and DE430 planetary ephemerides were used. Atmosphere and ocean de-aliasing effects were removed using the ECMWF and MOG2D (Carrere and Lyard, 2003) models. Ocean tides were accounted for using the GOT4.7 model with SCEQ model. The GIA effect was reduced using A Geruo et al. (2013) model. Table 2 lists all background models used for individual computing centers.

Table 2. Background models employed by the CSR, JPL and GSFC GRACE computing centers for the most recent releases of GRACE mascon solutions

Background models	GRACE analysis center		
	CSR	JPL	GSFC
Mean (static) gravity field	GGM05C	GIF48	GOCO-05S
3rd body ephemerides	DE430	DE421	DE430
Atmosphere and ocean de-aliasing	AOD1B (ECMWF+MPIOM)	AOD1B (ECMWF+OMCT)	AOD1B (ECMWF+MOG2D)
Ocean tides	GOT4.8+SCEQ	GOT4.7+SCEQ	GOT4.7+SCEQ
Solid Earth and pole tides	IERS2010	IERS2010	IERS2010
Degree-1 spherical harmonic coefficients	coefficients based on ocean and atmospheric models and GRACE coefficients for degrees 2 and higher (TN13a; Sun et al., 2016)	coefficients based on ocean and atmospheric models and GRACE coefficients for degrees 2 and higher (TN13c; Sun et al., 2016)	coefficients based on ocean and atmospheric models and GRACE coefficients for degrees 2 and higher (Sun et al., 2016)
Degree-2 spherical harmonic coefficients	coefficients replaced using SLR estimates (TN11; Cheng and Ries, 2017)	coefficients replaced using SLR estimates (TN11; Cheng and Ries, 2017)	coefficients replaced using SLR estimates (TN07; Cheng et al., 2013)

3. Methodology

To reduce noise included in the GRACE-based GGMs, we used two noise filtering methods: the anisotropic decorrelation filter DDK3 (Kusche, 2007; Kusche et al., 2009) and isotropic Gaussian filter (Wahr et al., 1998).

DDK filter has been extensively described in Kusche (2007) and Kusche et al. (2009). Few types of DDK filter exist: starting from DDK1 to DDK8, which are characterized by a decreasing radius of filter (Kusche et al., 2009). We chose the DDK3 filter. DDK1 and DDK2 filters have more constrains (Sakumura, 2014) than the DDK3 filter. Higher filters leave some part of noise unfiltered (Godah et al., 2015) due to smaller filter radius (Sakumura, 2014).

Gaussian smoothing depends on the position of the kernel and the maximum degree and order of spherical harmonic coefficients. The Gaussian averaging function was presented by Jekeli (1981) in his Eq. (59) and can be computed with recursion relations as:

$$W_0 = \frac{1}{2\pi}, \quad W_1 = \frac{1}{2\pi}\left[\frac{1+e^{-2b}}{1-e^{-2b}} - \frac{1}{b}\right], \quad W_{n+1} = -\frac{2n+1}{b}W_n + W_{n-1} \tag{1}$$

with:

$$b = \frac{\ln(2)}{\left(1 - \cos\left(\frac{r}{a}\right)\right)}, \tag{2}$$

where n is a maximum degree of spherical harmonic coefficients, r is a smoothing radius, b is a dimensionless parameter characterizing the smoothing process and a is an average Earth radius. Wahr et al. (1998) showed that the filter values decrease for large areas as degree and order of spherical harmonic coefficients increase. We used Gaussian filter with smoothing radius of 300 km, which is similar to the spatial smoothing provided by the DDK3 filter (Sakumura, 2014; Kusche et al., 2009).

Mascon solutions are provided in a form of gridded *TWS* values defined for a specific ranges of latitudes and longitudes. We convert the global sets of gridded *TWS* values provided by the CSR, JPL and GSFC computing centers into spherical harmonic coefficients C_{nm} and S_{nm} (which we refer to as "GRACE-M-based GGMs") using two-step procedure. Step (1): We calculate the dimensionless coefficients $\hat{C}_{nm}$ and $\hat{S}_{nm}$ defined in Eq. (11) of Wahr et al. (1998) using global set of $TWS(\theta, \lambda)$ with equations:

$$\hat{C}_{nm} = \frac{1}{R}\frac{1}{4\pi}\iint_{\sigma} TWS(\theta, \lambda)\overline{P}_{nm}(\cos\theta)\cos(m\lambda)\,\mathrm{d}\sigma, \tag{3}$$

$$\hat{S}_{nm} = \frac{1}{R}\frac{1}{4\pi}\iint_{\sigma} TWS(\theta, \lambda)\overline{P}_{nm}(\cos\theta)\sin(m\lambda)\,\mathrm{d}\sigma, \tag{4}$$

where θ is a colatitude, λ is a longitude, $R = 6378136.3$ m is the radius of the Earth, $\overline{P}_{nm}$ are fully normalized Legendre functions of degree n and order m. The $\mathrm{d}\sigma$ term equals to $\sin\theta\,\mathrm{d}\theta\,\mathrm{d}\varphi$ and means the basic area element. Step (2): Dimensionless coefficients $\hat{C}_{nm}$ and $\hat{S}_{nm}$ are converted to spherical harmonic coefficients C_{nm} and S_{nm} using (Wahr et al., 1998):

$$\{C_{nm}\} = \frac{3\rho_w}{\rho_e}\frac{1+k'_n}{2n+1}\{\hat{C}_{nm}\}, \tag{5}$$

$$\{S_{nm}\} = \frac{3\rho_w}{\rho_e}\frac{1+k'_n}{2n+1}\{\hat{S}_{nm}\}, \tag{6}$$

where $\rho_w = 1000\,\frac{\mathrm{kg}}{\mathrm{m}^3}$ is a water density, $\rho_e = 5496\,\frac{\mathrm{kg}}{\mathrm{m}^3}$ is a mean Earth's density, and k'_n is an elastic load Love number for degree n, provided by Farrell (1972). To stay consistent

with the GRACE-based GGMs, the global sets of $TWS(\theta, \lambda)$ values are converted to spherical harmonic coefficients up to d/o 96. Similar procedure is described by Wang et al. (2017b), where spherical harmonic coefficients obtained from gridded TWS values are used to estimate vertical deformations.

To characterize the variance of signal included in each degree n of the spherical harmonic coefficients, we estimate the square root of degree variance using the following formula (Sakumura, 2014):

$$\sigma_n^2 = \frac{1}{M} \sum_{k=1}^{M} \sum_{m=0}^{n} C_{nm}^2(t_k) + S_{nm}^2(t_k) \qquad (7)$$

where n and m means the degree and order of spherical harmonic coefficients for both GRACE-based GGMs and GRACE-M-based GGMs, k is the GRACE observations month, M is a total number of months investigated, and C_{nm} and S_{nm} are spherical harmonic coefficients. The square root of the degree variance is determined as an average of all months of GRACE observations available from each processing center.

4. Results and discussion

To present the variability of various RL06 GRACE-based GGMs, we compute the annual amplitude of TWS for the CSR, GFZ and JPL centers including unfiltered GRACE-based GGMs, and GRACE-based GGMs filtered using the Gaussian and DDK3 filters (Fig. 1). For unfiltered GRACE-based GGMs, evident north-south stripes can be noticed,
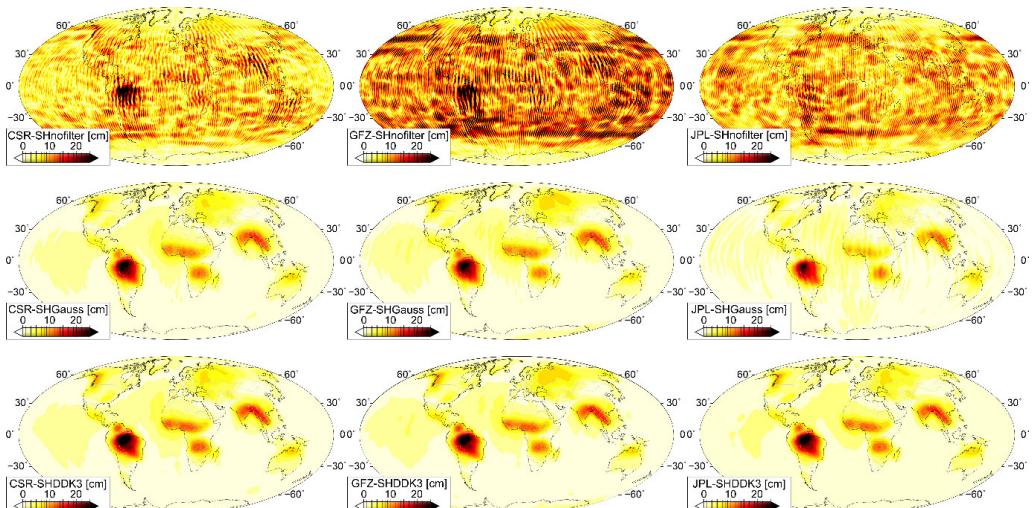
Fig. 1. Annual amplitude of TWS values obtained for RL06 GRACE-based GGMs provided by the CSR (left column), GFZ (middle column) and JPL (right column) centers. Maps present the estimates for no noise filtering applied (SHnofilter, top row), for fields filtered with Gaussian filter (SHGauss, middle row) and for fields filtered using decorrelation DDK3 filter (SHDDK, bottom row)

which cover the annual changes of *TWS*. For these unfiltered solutions, the CSR data are characterized by the weakest noise, while GFZ data are affected by the strongest noise. Both filtering methods allow to reduce the longitudinal stripes, yielding interpretation of GRACE-based GGMs. Spatial smoothing of GRACE observations using Gaussian filter reduces the annual amplitudes more than the DDK3 filter in all three solutions we use. Similarly to GRACE-based GGMs data, we also present the annual amplitude of *TWS* variations obtained for the most recent GRACE-M-based GGMs provided by the CSR, JPL and GSFC centers (Fig. 2). We notice that the use of mascons instead of spherical harmonic coefficients allows to retrieve more regional changes of *TWS*. For GRACE-M-based GGMs, we can observe regional annual amplitudes in Mexico, the High Plains Aquifers, north part of Australia and Caspian Sea regions, which is not possible for the GRACE-based GGMs. Larger *TWS* annual amplitudes were also obtained for GRACE-M-based GGMs for Alaska, North-West America and South-West Canada. Individual GRACE-M-based GGMs show few differences. For example, the *TWS* amplitudes are larger for European area for the CSR and JPL solutions than they are for the GSFC solution. The differences between solutions result from various data processing strategies and the use of different background models as listed in Tables 1 and 2. They may also arise from various mascon definitions and constraints made at the stage of noise reduction.
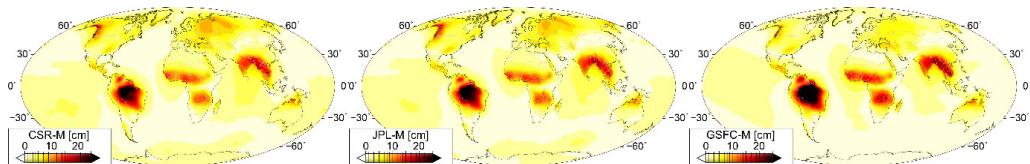
Fig. 2. Annual amplitude estimated for *TWS* changes obtained from GRACE mascon solutions provided by the CSR (left), JPL (middle) and GSFC (right) centers

We focused on the detailed analysis of data provided by different computing centers in two different data types. Research is carried out as an average for 163 months of GRACE Level-2 product provided by the CSR, GFZ and JPL computing centers and for 148 months of GRACE Level-2 product provided by the GSFC computing center for the GRACE-M-based GGMs.

Figure 3 presents unitless values of square root of degree variance of spherical harmonic coefficients values estimated using Eq. (7) for different GRACE solutions. We notice that signal variances are very similar for all solutions we investigate until degree 15. For higher degrees, i.e. from degree 15 and onward, errors in GRACE data start to dominate the signal amplitude, which was also observed by Save et al. (2012). Square root of degree variance obtained from unfiltered GRACE-based GGMs differ significantly from other datasets. This might be ascribed to the fact that unfiltered GRACE-based GGMs characterized by strong noise, observed as a discrepancy between those and other solutions from degree 20 onwards. High signal variance at lower degrees demonstrates that both GRACE-based GGMs and GRACE-M-based GGMs are able to detect large-scale temporal signals, related to global hydrological signal (Zhou
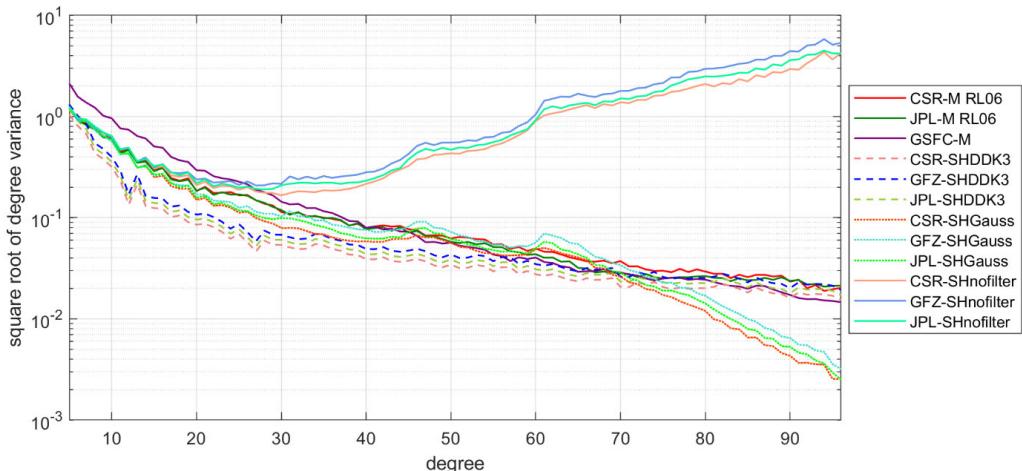
Fig. 3. Square root of the degree variance (unitless) of spherical harmonic coefficients values for degrees up to 96 estimated for various data types of GRACE solutions. Results are calculated as an average for 163 CSR, GFZ, JPL GRACE monthly solutions and for 148 GSFC GRACE monthly solutions. GRACE-based GGMs (SH) are presented for different filters: decorrelation filter DDK3 (SHDDK3, dashes lines) and Gaussian filter (SHGauss, dotted lines). Original GRACE-based GGMs, with no spatial smoothing applied (SHnofilter) as well as GRACE-M-based GGMs (M) are also plotted. Various colors stand for different analysis center whose data we use in this research: CSR (red curves), GFZ (blue curves), JPL (green curves) and GSFC (purple curve)

et al., 2018). Decreasing values of signals variance with an increasing degree concurs with the behavior of the geophysical models, i.e. hydrological and oceanographic models (Wahr et al., 1998). The strongest noise for unfiltered GRACE-based GGMs is found for the GFZ data, whereas the weakest noise is found for the CSR solution. The Gaussian filter (SHGauss) reduces the signal variance more than the DDK3 filter (SHDDK3). This is mainly observed by signal damping for degrees higher than 70 with the largest constrains for the CSR data. An increase in signal variance is observed for the GRACE-based GGMs filtered with Gaussian filter for degrees 45 and 60 for GRACE-based GGMs provided by all computing centers, which reflected as prominent north-south stripes in *TWS* global values. For all GRACE-based GGMs filtered with DDK3 we obtained almost identical variance changes. However, similar signal variance found for the CSR, GFZ and JPL GRACE-based GGMs is distributed differently into local signal and noise (Fig. 1). The DDK3 filter reduces the noise included in GRACE-based GGMs more than the Gaussian filter. Moreover, comparatively to GRACE-M-based GGMs, GRACE-based GGMs filtered with DDK3 filter contain less variance for low degrees up to 34, where the real geophysical signal is also restricted (Wouters and Schrama, 2007). These differences are probably caused by filtering strategy. Comparing the GRACE-based GGMs provided by different computing centers filtered with DDK3 and Gaussian filters, we noticed that the type of filter impacts the signals variance much more than the background models applied during data processing.

For GRACE-M-based GGMs provided by the CSR and JPL computing centers, we noticed similar values of degree variance for all examined degrees. Also, similar results for the CSR and JPL GRACE-M-based GGMs were obtained for the annual amplitudes presented in Figure 2. We showed that the GRACE-based GGMs provided by the GSFC is characterized by more rigorous degree variance constrains for high degrees. Furthermore, for degrees up to 40, the signal variance estimated for the GSFC GRACE-M-based GGMs is larger than the corresponding ones obtained from the CSR and JPL solutions (Fig. 3), which is observed as more pronounced large-scale signals in Figure 2. Signal variance estimated for GSFC GRACE-M-based GGMs data decreases with increasing degrees, but remains smaller than the JPL and CSR solutions for all degrees from 40 onwards. As a result, local changes in GSFC GRACE-M-based GGMs are poorly demonstrated than those for the JPL and CSR centers, which is noticed for global *TWS* values (Save et al., 2016; Loomis et al., 2019). Similar conclusions were presented by Loomis et al. (2019) for degree error variance estimated for the uncertainties of mascon solutions provided by the GSFC and JPL computing centers. They concluded that the GSFC GRACE-M-based GGMs have a greater leakage uncertainty than the JPL solution. The differences in signal variance between the CSR and JPL GRACE-M-based GGMs arise from method the computing centers employed to remove land-ocean signal leakage. They may also be caused by different background models used to remove the non-tidal ocean loading (as listed in Table 2). Moreover, in the case of GRACE-based GGMs filtered with Gaussian smoother and DDK3 filter, the differences in signal variance between the CSR, GFZ and JPL solutions arise mainly from the diversity of background models, i.e. the mean (static) gravity field model, as well as tidal and non-tidal ocean models (Table 1). However, those differences are minor. A drop in signal variance between 15 and 30 degrees for GRACE-based GGMs filtered with DDK3 and between 20 and 40 degrees for Gaussian filter may be partly related to the dependency of a filter on a degree (Han et al., 2005).

Similarly, to Save et al. (2016) and Watkins et al. (2015), we also obtained greater variance of signal for GRACE-M-based GGMs than for GRACE-based GGMs at all degrees we considered. An exception is for GRACE-based GGMs filtered with Gaussian filter near 45 and 60 degrees, caused by the filtering of stripping effects in GRACE monthly gravity field (Svehla, 2018). It can be noticed from Figure 3 that the GRACE-M-based GGMs contain more signal variance at all degrees than the GRACE-based GGMs do. It has already been noticed by Rodell et al. (2018) and Scanlon et al. (2018) as significant local signals visible on the *TWS* trend map, e.g. for Asia and South America regions, by Wang et al. (2017b) in case of Earth's crust vertical deformations in Greenland or by Watkins et al. (2015). Therefore, mascons solutions are more often used to enhance products that assimilate GRACE data (Houborg et al., 2012).

Now we focus on signal information contained in individual spherical harmonic coefficients C_{nm} and S_{nm}. Signal variance we presented in Figure 3 is similar for all computing centers and data types we use. Therefore, we take data provided by the CSR center as the reference due to weak noise occurring in the CSR GRACE-based GGMs (Fig. 1). Figure 4 presents gravity signal contained in each degree and order of spherical harmonic
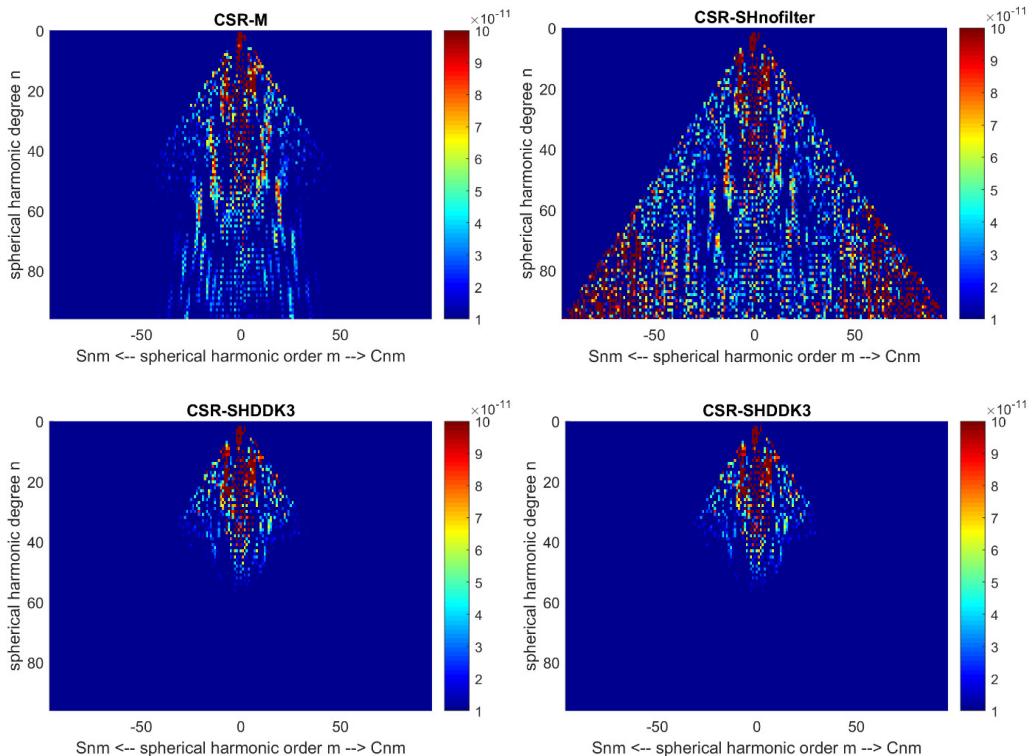
Fig. 4. Spherical harmonic coefficients plotted for the GRACE RL06 solution provided by the CSR comput-
ing center, which we assume as a reference. Results are calculated as an average for 163 GRACE monthly
solutions. They are plotted for: (1) GRACE-M-based GGMs estimated from mascon solution (CSR-M),
(2) for the unfiltered GRACE-based GGMs (CSR-SHnofilter), (3) for GRACE-based GGMs filtered with
the DDK3 filter (CSR-SHDDK3) and (4) for GRACE-based GGMs filtered with Gaussian filter (CSR-
SHGauss)

coefficients for both data types, i.e. GRACE-based GGMs as well as mascons converted
to the spherical harmonic coefficients (GRACE-M-based GGMs). We noted that for all
data forms provided by the CSR analysis center, the largest amount of information is con-
tained within the lowest harmonic degrees and orders. We noticed that unfiltered CSR
GRACE-based GGMs (CSR-SHnofilter) include more information in low and high de-
grees of spherical harmonic coefficients. However, the extreme values above degree and
order 60, mainly represent noise in observations. These values represent an unremoved
noise included in the GRACE observations (north-south stripes). For the GRACE-based
GGMs filtered using both DDK3 (CSR-SHDDK3) and Gaussian (CSR-SHGauss) fil-
ters, a similar distribution of signal content is observed. GRACE-based GGMs filtered
with the DDK3 filter contain more information at order 10 and above degree 40. In ad-
dition, GRACE-based GGMs provided by the CSR computing center and filtered using
the Gaussian filter have stronger noise for sectorial harmonics above 35 degree than data
filtered with DDK3 filter.

As shown in Figure 4, the CSR GRACE-M-based GGMs contain much more information than GRACE-based GGMs filtered with Gaussian and DDK3 filters. This is well demonstrated for coefficients of all orders above degree 60 and for all degrees between the orders 30 and 40. Such a large information contained in higher degrees allows a more reliable analyses of a short wave signal which is required in local hydrological or glaciological studies (Kusche, 2007). This feature has been also already shown by Watkins et al. (2015) and Scanlon et al. (2016). The difference between GRACE-M-based GGMs and GRACE-based GGMs smoothed with both the DDK3 and Gaussian filters arises from the reduction of the signal in the process of spatial filtering.

To assess the signal contained in other forms of data, we estimate the differences between GRACE-based GGMs and GRACE-M-based GGMs. We take here GRACE-based and GRACE-M-based GGMs estimated for GRACE solutions provided by the CSR computing center as a reference (Fig. 5). We noticed that unfiltered GRACE-based GGMs vary among computing centers for the higher spherical harmonic degrees and orders. For the GRACE-based GGMs provided by GFZ and JPL, smoothing the data with the DDK3 and Gaussian filters leaves similar signal information to the CSR GRACE-based GGMs. Slightly larger differences are noticed between the CSR and JPL GRACE-based GGMs filtered by the DDK3. For the DDK3 filter, similar results were obtained by Sakumura et al. (2014) for data from CSR, GFZ and JPL centres. For data from all three centers, the differences for the GRACE-based GGMs DDK3-filtered solution occur only up to the order of 10 and for the sectorial coefficients up to 30. For each Gaussian-filtered GRACE-based GGMs, the discrepancies can be noticed for the sectorial coefficients up to 70. These slight differences may result from the various parameters and background models employed during GRACE data processing.

For GRACE-M-based GGMs, the differences between data provided by all three computing centers are larger than those obtained from GRACE-based GGMs. They result from various geometrical and physical constraints used during the construction of mascons, i.e. their shape and size as well as different background models employed (Table 2). All the above manifest itself in the differences found for GRACE-based GGMs (Fig. 5), the signal variance (Fig. 3) and annual amplitudes (Fig. 2). The maximum discrepancies between CSR and JPL GRACE-M-based GGMs occur for the tesseral coef-
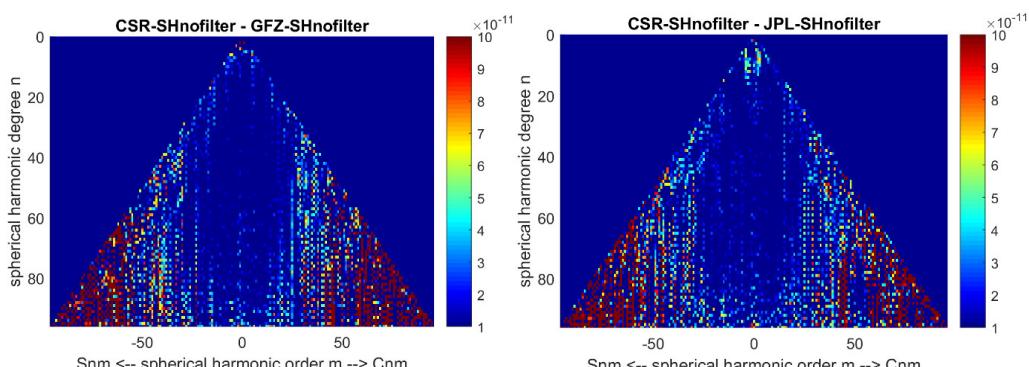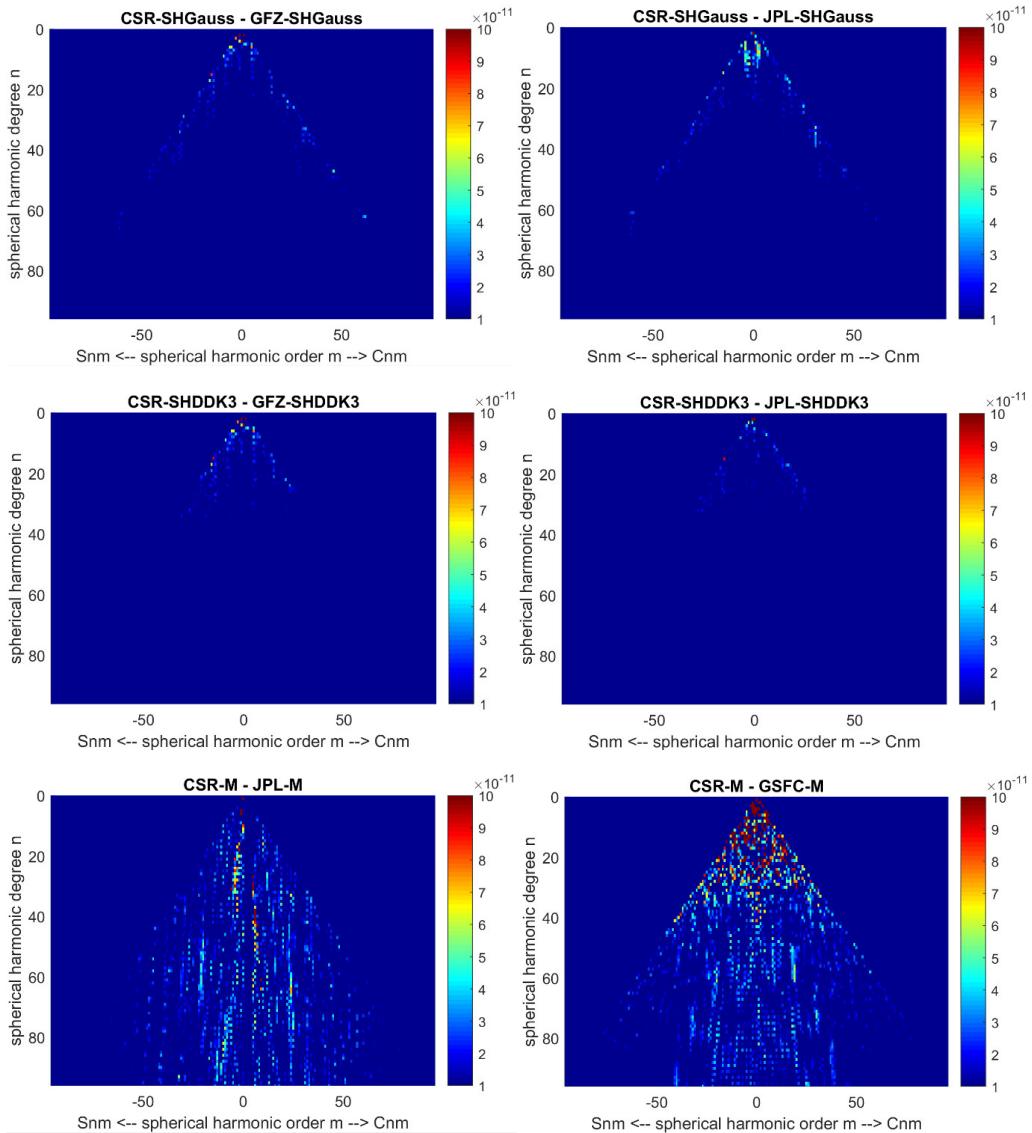
Fig. 5. Differences between average spherical harmonic coefficients for data provided by all computing centers. Results are calculated as an average for 163 CSR, GFZ, JPL GRACE monthly solutions and for 148 GSFC GRACE monthly solutions. Plotted are the differences between the CSR (reference) and the GFZ and JPL solutions of: (1) the unfiltered GRACE-based GGMs (first row), (2) the GRACE-based GGMs smoothed with the Gaussian smoother (second row), (3) the GRACE-based GGMs smoothed with the DDK3 filter (third row) and (4) the GRACE-M-based GGMs computed from the JPL and GSFC mascon solutions (fourth row)

ficients, mainly for low degrees and orders. The differences result, among others, from different methods assumed to reduce the signal leakage, as well as from the shape and the size of mascons. For GSFC GRACE-M-based GGMs data, the largest differences

with respect to the CSR solution result from a different approach of modelling leakage effects for the GSFC GRACE Level-2 product (Loomis et al., 2019). The same was also noticed for the signal variance (Fig. 3).

5. Summary and conclusions

In this study, we determine and compare the variance of signal contained in the most recent various GRACE solutions provided in two basic data forms: spherical harmonic coefficients (GRACE-based GGMs) and mass concentration blocks (mascons). The latter have been converted to the spherical harmonic coefficients (GRACE-M-based GGMs) for the comparison purposes. Our research proves that the proper choice of GRACE Level-2 products and the method of their filtering enables studying gravity field parameters in various spatial resolutions. We proved that GRACE-M-based GGMs are more appropriate to retrieve small scale changes, as shown for annual amplitude values; there are clear differences between GRACE-based and GRACE-M-based GGMs for Greenland, the High Plain Aquifers, Mexico and Madagascar areas. Additionally, for the GRACE-M-based GGMs the annual amplitudes are larger by 20-30% comparing to GRACE-based GGMs for areas of Alaska, North-West America and South-West Canada (Fig. 4). Degree variance and signal information contained in the GRACE solutions are compared for individual degrees and orders of spherical harmonic coefficients. We obtain the lowest signal variance for low spherical harmonic coefficients up to degree and order 34 for GRACE-based GGMs filtered with DDK3. It could be partly related to degree-dependency of the filter. The degree variance changes are similar up to maximum spherical harmonic coefficients for GRACE-based GGMs provided by all computing centers. GRACE-based GGMs provided by all computing centers (CSR, GFZ and JPL) and filtered using Gaussian filter are characterized by the lowest signal variance for the degrees above 70. We show that data filtering using the DDK3 filter leaves more information than the commonly applied Gaussian filter. We also demonstrate that despite a similar signal variance for Gaussian- and DDK3-filtered GRACE-based GGMs, the signal has different distribution for different centers. We show that despite almost identical degree variance values for all data centers filtered with DDK3 (Fig. 3), we obtain a different distribution of local mass changes. Moreover, the decreasing variance values presented in Figure 3 for all data with increasing degree concurs with the behavior of the geophysical models. Additionally, we show that in the case of GRACE-based GGMs, the method of filtering the observation noise has a greater impact on the final signal than various processing approaches and background models used. We demonstrate that the choice between GRACE-based GGMs and GRACE-M-based GGMs has also a significant impact on the calculated parameters of the gravity field (Figs. 1 and 2). This has been already noticed by Watkins et al. (2015) in the case of global water mass changes values and by Wang et al. (2017a) for the vertical deformations of the Earth's crust. The largest gravity signal is contained in spherical harmonic coefficients computed from the three available GRACE-M-based GGMs solutions, i.e. provided by the CSR, JPL and GSFC computing centers. The GSFC GRACE-M-based GGMs signal differs most

from the others. The differences between them are mainly due to their diverse shape, size and the various methods of eliminating signal leakage effects (Luthcke et al., 2013; Save et al., 2016; Watkins et al., 2015). Hence, it is difficult to assess the impact of the used various models on the ultimate signal due to their definition. Therefore, we showed that in comparison to GRACE-based GGMs, the GRACE-M-based GGMs allow users to perform analysis on smaller spatial scales due to much more signal information contained in the higher degrees, where the local hydrological and glaciological short wave signal is comprised.

Acknowledgments

References

A, Geruo, Wahr, J., and Zhong S. (2013). Computations of the viscoelastic response of a 3-D compressible Earth to surface loading: an application to Glacial Isostatic Adjustment in Antarctica and Canada. *Geophys. J. Int.*, 192, 557–572. DOI: 10.1093/gji/ggs030.

Andrews, S.B., Moore, P. and King, M.A. (2014). Mass change from GRACE: a simulated comparison of Level-1B analysis techniques. *Geophys. J. Int.*, 200(1), 503–518. DOI: 10.1093/gji/ggu402.

Bettadpur, S. (2018). GRACE 327-742 (CSR-GR-12-xx) (Gravity Recovery and Climate Experiment), UTCSR Level-2 Processing Standards Document (Rev. 5.0, April 18, 2018), (For Level-2 Product Release 0006), Center for Space Research, The University of Texas at Austin.

Bouman, J. and Fuchs, M.J. (2012). GOCE gravity gradients versus global gravity field models. *Geophys. J. In.*, 189(2), 846–850. DOI: 10.1111/j.1365-246X.2012.05428.x.

Bruinsma, S., Lemoine, J., Biancale, R. and Vales, N. (2010). CNES/GRGS 10-day gravity field models (release 2) and their evaluation. *Adv. Sp. Res.*, 45, 587–601. DOI: 10.1016/j.asr.2009.10.012.

Carrere, L. and Lyard F. (2003). Modeling the barotropic response of the global ocean to atmospheric wind and pressure forcing Comparisons with observations. *Geoph. Res. Lett.*, 30(6), 1275. DOI: 10.1029/2002GL016473.

Chambers, D.P. and Bonin, J.A. (2012). Evaluation of release-05 GRACE time variable gravity coefficients over the ocean. *Ocean Sci.*, 8(5), 859–868. DOI: 10.5194/os-8-859-2012.

Chen, J.L., Wilson, C.R. and Tapley, B.D. (2006). Satellite gravity measurements confirm accelerated melting of Greenland Ice Sheet. *Science*, 313, 1958–1960. DOI: 10.1126/science1129007.

Cheng, M. and Tapley, B.D. (2004). Variations in the Earth's oblateness during the past 28 years. *J. Geophys. Res.*, 109, B09402. DOI: 10.1029/2004JB003028.

Cheng, M.K. and Ries J.C. (2017). The unexpected signal in GRACE estimates of C20. *J. Geod.*, 91, 897–914. DOI: 10.1007/s00190-016-0995-5.

Dah-Ning, Y. (2018). GRACE 327-744 (Gravity Recovery and Climate Experiment), JPL Level-2 Processing Standards Document, For Level-2 Product Release 06 (June 1, 2018), Jet Propulsion Laboratory, California Institute of Technology.

Dahle, C., Flechtner, F., Murböck, M., Michalak, G., Neumayer, H., Abrykosov, O., Reinhold, A. and König, R. (2018). GRACE 327-743 (Gravity Recovery and Climate Experiment), GFZ Level-2 Processing Standards Document for Level-2 Product Release 06 (Rev. 1.0, October 26, 2018), (Scientific Technical Report STR – Data; 18/04), Potsdam: GFZ German Research Centre for Geosciences. DOI: 10.2312/GFZ.b103-18048.

Farrell, W.E. (1972). Deformation of earth by surface loads. *Rev. Geophys. Space Phys.*, 10, 761–797. DOI: 10.1029/RG010i003p00761.

Feng, W. (2019). GRAMAT: a comprehensive Matlab toolbox for estimating global mass variations from GRACE satellite data. *Earth Sci. Inform.*, 12, 389–404. DOI: 10.1007/s12145-018-0368-0.

Forsberg, R., Sørensen, L. and Simonsen, S. (2017). Greenland and Antarctica Ice Sheet Mass Changes and Effects on Global Sea Level. *Surv. Geophys.*, 38, 89–104. DOI: 10.1007/s10712-016-9398-7.

Godah, W., Szelachowska, M. and Krynski, J. (2015). On the selection of GRACE-based GGMs and a filtering method for estimating mass variations in the Earth system over Poland. *Geoinf. Issues*, 7(1), 5–14.

Han, S.-C., Shum, C.K., Jekeli, C., Kuo, C.-Y., Wilson, C. and Seo, K.-W. (2005). Non-isotropic filtering of GRACE temporal gravity for geophysical signal enhancement. *Geophys. J. Int.*, 163(1), 18–25. DOI: 10.1111/j.1365-246X.2005.02756.x.

Han, S.-C., Sauber, J., Luthcke, S.B., Ji, C. and Pollitz, F.F. (2008). Implications of postseismic gravity change following the great 2004 Sumatra-Andaman earthquake from the regional harmonic analysis of GRACE intersatellite tracking data. *J. Geophys. Res.: Solid Earth*, 113, B11413. DOI: 10.1029/2008JB005705.

Houborg, R., Rodell, M., Li, B., Reichle, R. and Zaitchik B. (2012). Drought indicators based on model assimilated GRACE terrestrial water storage observations. *Water Resour. Res.*, 48, W07525. DOI: 10.1029/2011WR011291.

Jekeli, C. (1981). Alternative methods to smooth the Earth's gravity field. *Technical Reports 327*, Department of Geodetic Science and Surveying, Ohio State Univ., Columbus, OH.

Kundu, S.N. (2016). GRACE, Climate Change and Future Needs: A Brief Review. *J. Climatol Weather Forecasting*, 4:179. DOI: 10.4172/2332-2594.1000179.

Kusche J. (2007). Approximate decorrelation and non-isotropic smoothing of time-variable GRACE-type gravity field models. *J. Geod.*, 81/11, 733-749. DOI: 10.1007/s00190-007-0143-3.

Kusche, J., Schmidt, R., Petrovic, S. and Rietbroek, R. (2009). Decorrelated GRACE time-variable gravity solutions for science by GFZ, and their validation using a hydrological model. *J. Geod.*, 83, 903–913. DOI: 10.1007/s00190-009-0308-3.

Loomis, B.D., Luthcke, S.B. and Sabaka, T.J. (2019). Regularization and error characterization of GRACE mascons. *J. Geod.*, 93(9), 1381–1398. DOI: 10.1007/s00190-019-01252-y.

Luthcke, S.B., Arendt, A.A., Rowlands, D.D, McCarthy, J.J. and Larsen C.F. (2008). Recent glacier mass changes in the Gulf of Alaska region from GRACE mascon solutions. *J. Glaciol.*, 54, 767–77. DOI: 10.3189/002214308787779933.

Luthcke, S.B., Sabaka, T.J., Loomis, B.D., Arendt, A.A., McCarthy, J.J. and Camp, J. (2013). Antarctica, Greenland and Gulf of Alaska land ice evolution from an iterated GRACE global mascon solution. *J. Glaciol.*, 59(216), 613–631. DOI: 0.3189/2013JoG12J147.

Muller, P.M. and Sjögren, W.L. (1968). Mascons: Lunar Mass Concentrations. *Science*, 161(3842), 680–684. DOI: 10.1126/science.161.3842.680.

Nair, A.S. and Indu, J. (2018). Utilizing GRACE and GLDAS data for estimating groundwater storage variability over the Krishna Basin. *ISPRS Ann. Photogramm., Remote Sens. Spatial Inf. Sci.*, IV-5, 129–136. DOI: 10.5194/isprs-annals-IV-5-129-2018.

Peidou, A. and Pagiatakis, S. (2020). Stripe Mystery in GRACE Geopotential Models Revealed. *Geophys. Res. Lett.*, vol. 47, issue 4, DOI: 10.1029/2019GL085497.

Peltier, W.R. (2004). Global Glacial Isostasy and the Surface of the Ice-Age Earth: The ICE-5G (VM2) model and GRACE. *Annu. Rev. Earth Planet. Sci.*, 32, 111–149. DOI: 10.1146/annurev.earth.32.082503.144359.

Peltier, W.R., Argus, D.F. and Drummond, R. (2018). Comment on "An Assessment of the ICE-6G_C (VM5a) Glacial Isostatic Adjustment Model" by Purcell et al. *J. Geophys. Res: Solid Earth*, 123, 2019–2018. DOI: 10.1002/2016JB01384.

Ray, R., Steinberg, D., Chao, B. and Cartwright, D. (1994). Diurnal and semidiurnal variations in the Earth's rotation rate induced by ocean tides. *Sci.*, 264, 830–832. DOI: 10.1126/science.264.5160.830.

Rexer, M., Pail R., Fecher T. and Meyer U. (2014). Time Variable Gravity: Contributions of GOCE Satellite Data to Monthly and Bi-monthly GRACE Gravity Field Estimates, Gravity, Geoid and Height Systems. *Int. Assoc. Geod. Symp. Series*, 141. DOI: 10.1007/978-3-319-10837-7_5.

Rodell, M., Famiglietti, J.S., Wiese, D.N., Reager, J.T., Beaudoing, H.K., Landerer, F.W. and Lo, M.-H. (2018). Emerging trends in global freshwater availability. *Nature*, 557(7707), 651–659. DOI: 10.1038/s41586-018-0123-1.

Rowlands, D.D., Luthcke, S.B., McCarthy, J.J., Klosko, S.M., Chinn, D.S., Lemoine, F.G., Boy, J.-P. and Sabaka, T.J. (2010). Global mass flux solutions from GRACE: a comparison of parameter estimation strategies – mass concentrations versus Stokes coefficients. *J. Geophys. Res*, 115:B01403. DOI: 10.1029/2009JB006546.

Sabaka, T.J., Rowlands, D.D. Luthcke, S.B. and Boy J.P. (2010). Improving global mass flux solutions from GRACE through forward modeling and continuous time-correlation. *J. Geophys. Res*, DOI: 10.1029/2010JB007533.

Sakumura, C. (2014). GRACE Technical Note 10 (CSR-GR-14-01) Gravity Recovery and Climate Experiment, Comparison of Degree 60 and Degree 96 Monthly Solutions, (May 5, 2014). Center for Space Research, The University of Texas at Austin.

Sakumura, C., Bettadpur, S. and Bruinsma S. (2014). Ensemble prediction and intercomparison analysis of GRACE time-variable gravity field models. *Geophys. Res. Lett.*, 41, 1389–1397. DOI: 10.1002/2013GL058632.

Save, H., Bettadpur, S. and Tapley B.D. (2012). Reducing errors in the GRACE gravity solutions using regularization. *J. Geod.*, 86(9), 695–711. DOI: 10.1007/s00190-012-0548-5.

Save, H., Bettadpur, S. and Tapley B.D. (2016). High-resolution CSR GRACE RL05 mascons. *J. Geophys. Res*, 121, 7547–5769. DOI: 10.1002/2016JB013007.

Scanlon, B.R., Zhang, Z., Save, H., Wiese, D.N., Landerer, F.W., Long, D., Longuevergne, L. and Chen, J. (2016). Global evaluation of new GRACE mascon products for hydrologic applications. *Water Resour. Res.*, 52(12), 9412–9429. DOI: 10.1002/2016wr019494.

Scanlon, B.R., Zhang, Z., Save, H., Sun, A.Y., Müller S.H., van Beek, L.P.H., Wiese D.N., Wada, Y., Long, D., Reedy, R.C., Longuevergne, L., Döll, P. and Bierkens, M.F.P. (2018). Global models underestimate large decadal declining and rising water storage trends relative to GRACE satellite data. *Proc. Natl. Acad. Sci.*, 115(6), E1080–E1089. DOI: 10.1073/pnas.1704665115.

Sun, Y., Riva, R. and Ditmar P. (2016). Optimizing estimates of annual variations and trends in geocenter motion and J2 from a combination of GRACE data and geophysical models. *J. Geophys. Res: Solid Earth*, 121. DOI: 10.1002/2016JB013073.

Svehla, D. (2018). Geomatrical Theory of Satellite Orbits and Gravity Field. Doctoral Thesis accepted by the Technische Universität München, Munich, Germany. Section 28.7. Temporal Variations in the Orientation of the Tri-Axial Earth's Ellipsoid and Low-Degree Sectorial Harmonics, 469–476.

Tapley, B.D., Bettadpur, S., Watkins, M. and Reigber, C. (2004). The gravity recovery and climate experiment: Mission overview and early results. *Geophys. Res. Lett.*, 31(9). DOI: 10.1029/2004gl019920.

Wahr, J., Molenaar, M. and Bryan F. (1998). Time variability of the Earth's gravity field: Hydrological and oceanic effects and their possible detection using GRACE. *J. Geophys. Res.*, 103, 30205–30229. DOI: 10.1029/98JB02844.

Wahr, J., Swenson, S. and Velicogna, I. (2006). Accuracy of GRACE mass estimates. *Geophys. Res. Lett.*, 33, L06401. DOI: 10.1029/2005GL025305.

Wang, L., Chen, Ch., Du, J. and Wang T. (2017a). Detecting seasonal and long-term vertical displacement in the North China Plain using GRACE and GPS. *Hydrol. Earth Syst. Sci.*, 21, 2905–2922. DOI: 10.5194/hess-21-2905-2017.

Wang, S.-Y., Chen, J.L., Wilson, C.R., Li, J. and Hu, X. (2017b). Reconciling GRACE and GPS estimates of long-term load deformation in southern Greenland. *Geophys. J. Int*, 212, 1302–1313. DOI: 10.1093/gji/ggx473.

Watkins, M.M., Wiese, D.N., Yuan, D.-N., Boening, C. and Landerer, F.W. (2015). Improved methods for observing Earth's time variable mass distribution with GRACE using spherical cap mascons. *J. Geophys. Res: Solid Earth*, 120(4), 2648–2671. DOI: 10.1002/2014jb011547.

Wouters, B. and Schrama, E.J.O. (2007). Improved accuracy of GRACE gravity solutions through empirical orthogonal function filtering of spherical harmonics. *Geophys. Res. Lett.*, 34, L23711. DOI: 10.1029/2007GL032098.

Zhou, H., Luo, Z., Tangdamrongsub, N., Zhou, Z., He, L., Xu, Ch., Li, Q., and Wu, Y. (2018). Identifying Flood Events over the Poyang Lake Basin Using Multiple Satellite Remote Sensing Observations. Hydrological Models and In Situ Data. *Remote Sens.*, 10(5), 713. DOI: 10.3390/rs10050713.